RESEARCH PAPER

A prediction of in vivo mechanical stresses in blood vessels using thermal expansion method and its application to hypertension and vascular stenosis

Shaoxiong Yang[1] · Lucy T. Zhang[2,3] · Cheng Hua[4] · Yunqiao Liu[1] · Jingdong Tang[5] · Xiaobo Gong[1,6] · Zonglai Jiang[7]

Abstract

Mechanical stimuli play critical roles in cardiovascular diseases, in which in vivo stresses in blood vessels present a great challenge to predict. Based on the structural–thermal coupled finite element method, we propose a thermal expansion method to estimate stresses in multi-layer blood vessels under healthy and pathological conditions. The proposed method provides a relatively simple and convenient means to predict reliable in vivo mechanical stresses with accurate residual stress. The method is first verified with the opening-up process and the pressure-radius responses for single and multi-layer vessel models. It is then applied to study the stress variation in a human carotid artery at different hypertension stages and in a plaque of vascular stenosis. Our results show that specific or optimal residual stresses exist for different blood pressures, which helps form a homogeneous stress distribution across vessel walls. High elastic shear stress is identified on the shoulder of the plaque, which contributes to the tearing effect in plaque rupture. The present study indicates that the proposed numerical method is a capable and efficient in vivo stress evaluation of patient-specific blood vessels for clinical purposes.

Keywords Cardiovascular disease · In vivo stress · Multi-layer vessel structure · Hypertension · Stenosed vessel

✉ Xiaobo Gong
  x.gong@sjtu.edu.cn

1   Key Laboratory of Hydrodynamics (Ministry of Education), Department of Engineering Mechanics, School of Naval Architecture, Ocean and Civil Engineering, Shanghai Jiao Tong University, Shanghai 200240, China

2   Department of Mechanical, Aerospace and Nuclear Engineering, Rensselaer Polytechnic Institute, Troy, NY 12180, USA

3   School of Mechanical Engineering, Tianjin University of Science and Technology, Tianjin 300222, China

4   Department of Aeronautics and Astronautics, Fudan University, Shanghai 200433, China

5   Vascular Surgery Department, Shanghai Pudong Hospital, Fudan Affiliated Pudong Medical Center, Shanghai 200120, China

6   Collaborative Innovation Center for Advanced Ship and Deep Sea Exploration, School of Naval Architecture, Ocean and Civil Engineering, Shanghai Jiao Tong University, Shanghai 200240, China

7   Institute of Mechanobiology and Biomedical Engineering, School of Life Sciences and Biotechnology, Shanghai Jiao Tong University, Shanghai 200240, China

1 Introduction

Medical practitioners are realizing that variations of the mechanical stress beyond normal biological conditions are closely associated with vascular remodeling and pathological changes [1–3]. In order to explore a better understanding of the stress-modulated remodeling of vascular tissues, it is important to analyze the variations of in vivo mechanical stress quantitatively. A lack of feasible approaches to measure in vivo stress distribution of a vascular wall, prediction based on continuum mechanics provides a credible solution [4].

A vascular wall is not stress-free even in the absence of an external load such as blood pressure. The existence of residual stress in unloaded blood vessels was confirmed in 1980s [5]. Because of the nonlinear mechanical behavior of

vascular tissues, it is of crucial importance to estimate the residual stress properly for further mechanical analysis.

As most residual stress of a blood vessel releases after it is cut in radial directions with the opening of the vessel [6], many studies set up the residual stresses through a reversed process by folding the opened-up sectors. This conventional reversed numerical approach is called the "opening angle method" [7–10]. It was proven by Delfino et al. [7] that the opening angle method helped predict the maximum stress in a human carotid bifurcation much more reasonably comparing to those without considering the residual stress. However, the opening angle method often causes discontinuous stress distribution or non-matching stress at the rejoined sections when without a precise "sealing" at the cutting ends [9]. Particularly when the multi-layer structure of blood vessels is considered, separate bending loads are necessary to fold each layer with different opening angles [8].

Most recently, residual stresses are developed through intermediate ways for blood vessels in pathological conditions. In their work, Polzer et al. [11] modeled the residual stress with a volumetric tissue growth method that allows a fast stress prediction of the abdominal aortic aneurysm (AAA). The residual stress is estimated by adjusting the increment of growth iteratively, based on the hypothesis that the presence of residual stress leads to a homogeneous stress distribution across the vascular wall [12]. Although the homogeneous stress hypothesis simplifies the stress analysis of blood vessels, it is not clear whether this hypothesis is feasible to model vessels realistically with complicated three-dimensional geometries. A generalized prestressing algorithm (GPA) was introduced by Weisbecker et al. [13] for predicting the stress distributions in the loaded vessel models reconstructed from the in vivo medical imaging data. This algorithm creates a prestressing configuration without changing the initial geometry by resetting the calculated displacement to zero during every converged iterative solution. Using GPA, Pierce et al. [14] successfully applied measured residual stresses directly into the patient-specific simulations of AAAs. This approach was expected to improve the reliability of stress predictions within the vessel walls with aneurysms. But Pierce et al. introduced the residual stress into a pressure loaded geometry rather than an unloaded one. The possible effects of the geometry mismatch on wall stress predictions need to be further quantified.

In this work, we proposed a thermal expansion method, which is a relatively simple and convenient approach to rebuild the residual stress for healthy and stenosed vessels. The method applies the residual strain field onto a blood vessel with known given opening angles by introducing the analytically solved thermal expansion. It greatly improves the reliability in predicting in vivo stress in the vessel wall under different physiological conditions, which allows us to evaluate and examine in vivo stress in the cases of vessels undergoing hypertension and complicated-shaped vessels with stenosis. For stenosed vessels, evaluating the mechanical stress is of critical importance on the prediction of plaque rupture, but few studies have been reported with residual stress taken into account [15]. Using our developed approach, one application is to estimate in vivo stress of stenosed vessels that can further predict plaque rupture.

The paper is organized as follows: the thermal expansion method is introduced in Sect. 2. The proposed method is verified for a range of opening angles and multi-layer models in Sect. 3. In Sect. 4, the stress variations of blood vessels under several selected blood pressures representing hypertensive conditions are investigated using the proposed method. The in vivo stress distribution of a stenosed vessel during a cardiac cycle is also analyzed, and implications on plaque rupture are discussed. Finally, conclusions and future work are presented in Sect. 5.

2 Numerical method

2.1 Thermal expansion method

Configurations adopted for the present methods are illustrated in Fig. 1. In Fig. 1a, a vessel at an unloaded state (without any external load) Ω_1, which is cut in a radial direction (along the dashed line) results in a relaxed stress-free state Ω_0 with an opening angle of Φ_0. Another virtual intact blood vessel in a stress-free configuration Ω_0^* is set up, as shown in Fig. 1b, which serves as a reference configuration. By introducing a thermal expansion into the reference configuration Ω_0^*, we achieve an expected unloaded configuration Ω_1 with residual stress distributed in the vessel. The unloaded configuration is slightly different from the desired configuration of Ω_1 due to practical and numerical errors; therefore, we denote it as Ω_1'. The corresponding discrete points represented in the model are also labeled as $\boldsymbol{x}'$ instead of $\boldsymbol{x}$.

For a simple illustration of the method, a straight blood vessel is used and treated as a cylindrical tube with known opening angles. The analytical evaluation of the residual strain is briefly introduced as follows.

Taking the stress-free state in Fig. 1a as the reference configuration, $\boldsymbol{X} \in (R, \Theta, Z)$, the deformation gradient tensor $\boldsymbol{F}$ for $\boldsymbol{x} \in (\rho, \vartheta, \zeta)$ is formulated in cylindrical coordinates as

$$\boldsymbol{F}(\boldsymbol{X}) = \frac{\partial \boldsymbol{x}(\boldsymbol{X})}{\partial \boldsymbol{X}} = \begin{bmatrix} \frac{\partial \rho}{\partial R} & \frac{1}{R}\frac{\partial \rho}{\partial \Theta} & \frac{\partial \rho}{\partial Z} \\ \rho\frac{\partial \vartheta}{\partial R} & \frac{\rho}{R}\frac{\partial \vartheta}{\partial \Theta} & \rho\frac{\partial \vartheta}{\partial Z} \\ \frac{\partial \zeta}{\partial R} & \frac{1}{R}\frac{\partial \zeta}{\partial \Theta} & \frac{\partial \zeta}{\partial Z} \end{bmatrix} = \begin{bmatrix} \frac{\partial \rho}{\partial R} & 0 & 0 \\ 0 & \frac{\pi\rho}{\Theta_0 R} & 0 \\ 0 & 0 & \Lambda \end{bmatrix},$$

(1)
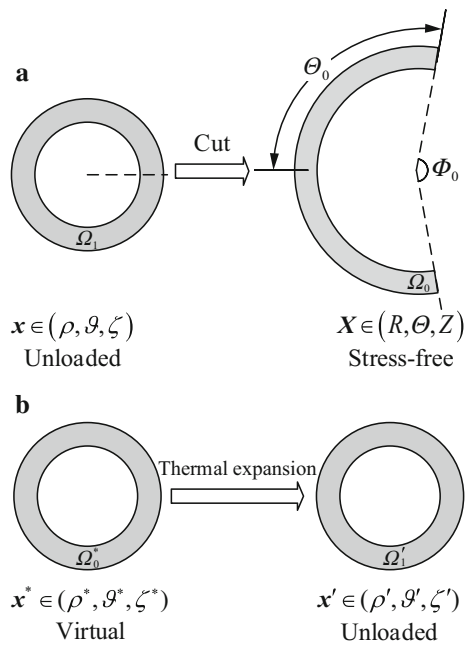
Fig. 1 **a** The release of residual stress is illustrated by cutting a blood vessel in an unloaded configuration Ω_1 along a radial direction (as shown by the dashed line), which results in an opened-up sector in the stress-free configuration Ω_0 with an opening angle Φ_0, where $\Theta_0 = \pi - \Phi_0/2$. **b** The generation of a blood vessel in an unloaded configuration Ω_1' with residual stress from a zero-stress blood vessel in a virtual configuration Ω_0^* through a thermal expansion process

where $\rho = \rho(R)$, $\vartheta = \pi \Theta/\Theta_0$ and $\zeta = \Lambda Z$. Λ is the axial stretch ratio, which is often assumed as $\Lambda = 1$ for plane strain [6]. The circumferential stretch ratio is evaluated as $\lambda_\vartheta = \pi \rho/(\Theta_0 R)$, and the circumferential residual strains $\varepsilon_{\vartheta i}$ and $\varepsilon_{\vartheta o}$ (with the subscripts "i" and "o" denote the inner and outer walls, respectively) are written as

$$\varepsilon_{\vartheta i} = \pi \rho_i/(\Theta_0 R_i) - 1, \tag{2}$$

$$\varepsilon_{\vartheta o} = \pi \rho_o/(\Theta_0 R_o) - 1. \tag{3}$$

Incompressibility of blood vessels requires $\det \boldsymbol{F} = 1$, so Eq. (1) leads to

$$\partial \rho/\partial R = \Theta_0 R/(\pi \rho). \tag{4}$$

The integration of Eq. (4), i.e. $\int_{\rho_i}^{\rho_o} \rho \mathrm{d}\rho = \int_{R_i}^{R_o} \frac{\Theta_0 R}{\pi} \mathrm{d}R$, yields

$$\rho_o^2 - \rho_i^2 = \Theta_0(R_o^2 - R_i^2)/\pi. \tag{5}$$

Following Holzapfel et al. [16], neglecting the variation of the thickness of the vessel wall from the stress-free state to the unloaded state, the inner and outer radii satisfy

$$\rho_o - \rho_i = R_o - R_i. \tag{6}$$

By solving Eqs. (5) and (6) for ρ_i, ρ_o with given geometries of the vessel R_i, R_o, and Φ_0, the inner and outer circumferential residual strains $\varepsilon_{\vartheta i}$ and $\varepsilon_{\vartheta o}$ are obtained from Eqs. (2) and (3).

For a single-layer vessel model, we assume that ε_ϑ varies linearly across the wall thickness

$$\varepsilon_\vartheta (\rho) = \varepsilon_{\vartheta i} + \frac{\rho - \rho_i}{\rho_o - \rho_i}(\varepsilon_{\vartheta o} - \varepsilon_{\vartheta i}). \tag{7}$$

For a multi-layer vessel model, a different linear distribution of the strain can be applied within each single layer similarly as Eq. (7).

By performing a thermal expansion process, the circumferential residual strain is mapped onto the unloaded vessel started from a virtual stress-free vessel, as illustrated in Fig. 1b. With the small deformation assumption for the expansion process, the virtual geometry is set to be the same as the unloaded geometry with negligible errors, i.e. $\rho^* \approx \rho$. The circumferential residual strain ε_ϑ in Eq. (7) is formulated as

$$\varepsilon_\vartheta (\rho^*) = -\alpha \Delta T(\rho^*), \tag{8}$$

and

$$\Delta T(\rho^*) = -\frac{1}{\alpha}\left[\varepsilon_{\vartheta i} + \frac{\rho^* - \rho_i^*}{\rho_o^* - \rho_i^*}(\varepsilon_{\vartheta o} - \varepsilon_{\vartheta i})\right]. \tag{9}$$

here, ρ^* is the radial distance in the virtual stress-free configuration; $\Delta T(\rho^*)$ in Eqs. (8) and (9) is the target temperature difference, which also varies linearly as a function of the radial distance ρ^*; α is the artificial thermal expansion coefficient of the vessel which pairs with ΔT to satisfy the circumferential residual strain $\varepsilon_\vartheta (\rho^*)$ as Eq. (8). By defining a proper temperature difference $\Delta T(\boldsymbol{x}^*)$ in its virtual configuration Ω_0^*, the thermal strain field $\varepsilon(\boldsymbol{x}')$ in the unloaded configuration Ω_1' is ensured to reproduce the residual strain field $\varepsilon(\boldsymbol{x})$. Once the residual strain is properly reproduced, further loading can be applied to obtain in vivo stress distributions in the vessel.

2.2 Practical procedure for rebuilding in vivo stress distributions in finite elements

In practice, the in vivo stress of a blood vessel using the thermal expansion method is estimated with finite elements in five steps:

(1) Generate a discretized mesh for the virtual or a stress-free reference configuration Ω_0^*. The two ends of the vessel are fixed in both circumferential and axial directions, but are allowed to expand freely in the radial direction. Keep these boundary conditions throughout the procedures unless specified otherwise.

Table 1 Blood vessels used in the present work with the reference geometries and constitutive relations

Vessel model	ρ_i^*(mm)	ρ_o^*(mm)	Opening angle		λ_z	Constitutive relation	Reference vessel type
Single-layer	3.1	4	$\Phi_0 = 100°$		1.1	Nonlinear isotropic [16,21]	Human carotid
Two-layer	1.725	2.527	$\Phi_{0M} = 160°$,	$\Phi_{0A} = 120°$	1.1	Nonlinear anisotropic [8]	Human coronary
Two-layer	0.71	1.10	$\Phi_{0M} = 160°$,	$\Phi_{0A} = 160°$	1.7	Nonlinear anisotropic [16]	Rabbit carotid

ρ_i^* and ρ_o^* are the inner and outer radii in virtual configuration; The subscripts "M" and "A" denote the media and adventitia layers, respectively; λ_z is the axial stretch ratio in loaded configuration

(2) Evaluate residual strains analytically at the inner and outer walls using Eqs. (2) and (3). Choose an artificial thermal expansion parameter for the vessel and obtain temperature differences for all discrete nodal points using Eq. (9).

(3) Apply the temperature difference onto each node in the virtual configuration Ω_0^*. Thermal strains on all nodal points are updated to unloaded state Ω_1' gradually through the thermal expansion of the materials as Eq. (8).

(4) Apply a uniform axial extension to represent a physiological loading by replacing the axial constraints for the nodes on one end with a specific axial stretch displacement $U_z = L\lambda_z$, where λ_z is the axial stretch ratio, L is the axial length of the model in the unloaded state.

(5) Apply an internal pressure as a blood pressure to the inner wall of the vessel.

For vessels with more complicated geometries such as stenosed vessels, the present method is also accessible with proper assumptions. Pathology studies show that the formation of a plaque at the inner wall mainly results from the accumulation of fatty substances, calcium and metabolic waste of cells beneath epithelial cells [17,18]. During the growth of the plaque, a stress distribution in the plaque appears as well. Based on the continuum mechanics, the variation of mechanical stress should be continuous across the stenosed wall from the inner wall of the vessel where the plaque starts growing. Therefore, we assume the stress of the plaque is consistent with its substrate of the inner wall at the interface between the plaque and vessel, and the stress inside plaque decreases gradually towards the surface to blood streams. In order to simulate the in vivo stress distribution in a stenosed vessel, we attached a plaque onto the inner wall of a straight tube geometrically and set boundary conditions for the two ends of the tube as described in step 1. According to steps 2 and 3, we calculated the temperature differences for the straight tube with known opening angles, and applied them on corresponding nodal points. While doing so, the same temperature difference as in the inner wall was added into the plaque. Through a thermal expansion process, we obtained a prestressed stenosed vessel. Finally, following steps 4 and 5, we rebuilt the in vivo stress of the stenosed vessel under
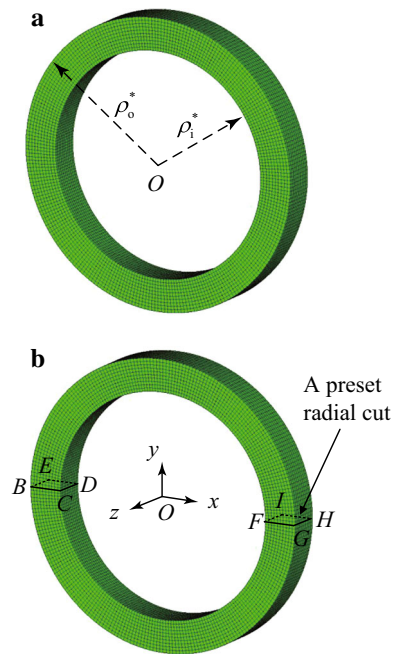
Fig. 2 a Discretized meshes of blood vessels at virtual state. **b** An illustration of a model with a preset radial cut, which is used to simulate the opening-up process. *BCDE* is the surface on which the constraints are adopted to eliminate the rigid body motion, and *FGHI* presents a radial cut which detaches the mesh to release the residual stress during the opening-up process

physiological loading conditions. The plaques often consist of different components [19,20], and stress distributions inside plaques are often non-uniform. In the present study, for demonstrating the proposed method, we adopted homogeneous assumptions for the plaque for simplicity. If the detailed stress concentrations of the plaque are of interest, the detailed material properties of the plaque are required, and more complicated contact conditions need to be introduced.

Similarly, this approach is also applicable for vessels with bifurcations. In such cases, separate thermal expansion is necessary to form the residual stress of each branch, and harmonic average can be used for the joint parts of two branches. Vessels with bifurcations will be included in our future studies.
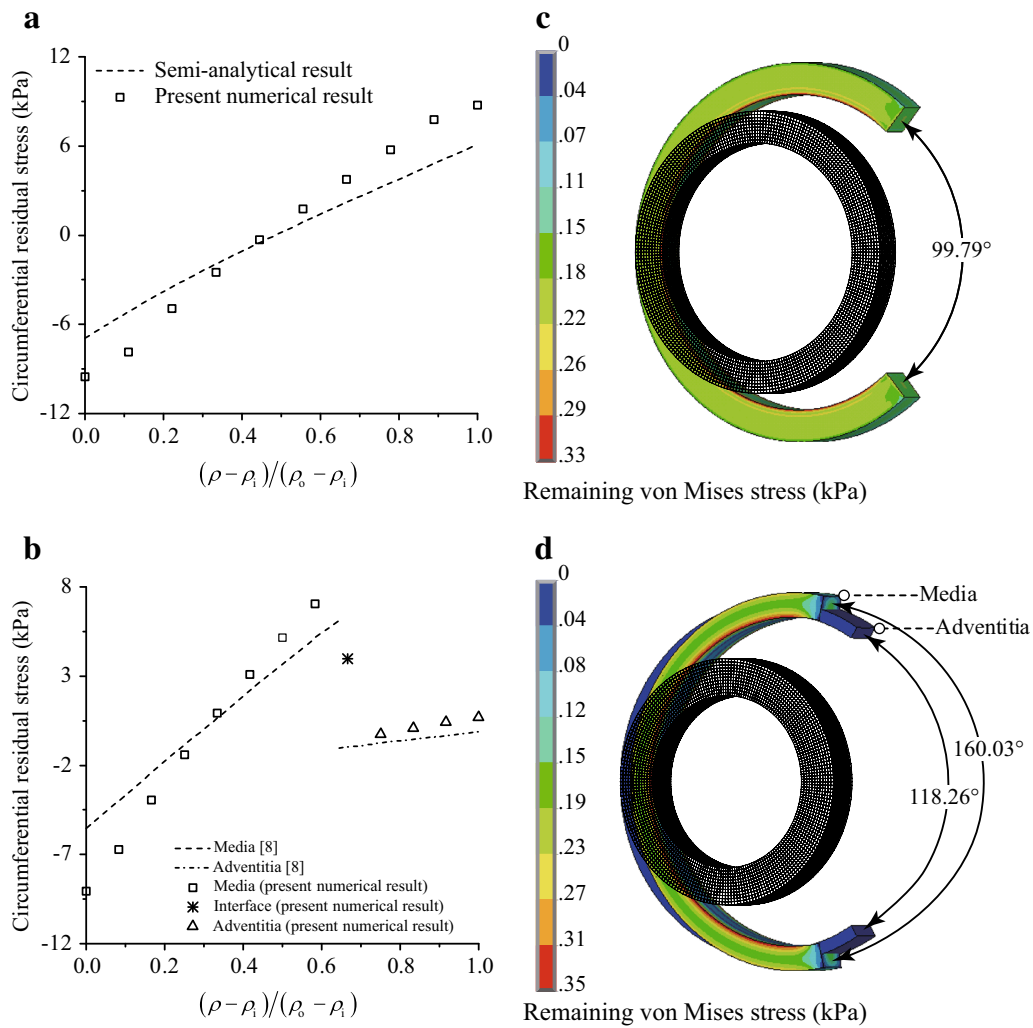
Fig. 3 The distributions of the circumferential residual stress across the wall (**a**, **b**), the opening angles and remaining von Mises stresses at the opened-up states (**c**, **d**). **a** For the single-layer model with reference opening angle $\Phi_0 = 100°$. **b** For the two-layer model with reference opening angles $\Phi_{0M} = 160°$ and $\Phi_{0A} = 120°$ for media layer and adventitia layer, respectively. The shadows show the unloaded states of the vessels as reference configurations to the opened-up configurations. Dashed line and dash-dotted line stand for the reference results, and discretized symbols (squares, star, and triangles) for the numerical results

3 Verification and error analysis

A thorough verification of the proposed thermal expansion method in reproducing accurate residual stress is done in this study. Three general types of blood vessels, single and multi-layer vessels, are referred to in the literature. They are human carotid artery [16,21], human coronary artery [8] and rabbit carotid artery [16]. Table 1 lists the corresponding geometrical data and material models.

For a single-layer vessel model of human carotid arteries, the constitutive relation proposed by Demiray [21] is used as Eq. (10), which presents the stiffening effects of vessels with the increase of blood pressure.

$$W = \frac{a}{b} \left\{ \exp\left[\frac{b}{2} \left(\bar{I}_1 - 3 \right) \right] - 1 \right\}, \tag{10}$$

Table 2 Error analysis on volume change

Vessel model	ρ_i^*(mm)	ρ_o^*(mm)	ρ_i'(mm)	ρ_o'(mm)	$\Delta V / V$
Single-layer	3.1	4	3.1099	4.0093	0.204%
Two-layer	1.725	2.527	1.7327	2.5329	0.095%

ρ_i' and ρ_o' are the numerical radii in unloaded configuration. $\Delta V / V$ is the ratio of volume change after the expansion process

in which $\bar{I}_1$ is the first invariant of the modified left Cauchy–Green tensor $\bar{b} = \bar{F}\bar{F}^T$, where the deformation gradient $F = \left(J^{1/3} I \right) \bar{F} = J^{1/3} \bar{F}$ and $J = \det F$. Following Holzapfel et al. [16], the parameters in this study are set as $a = 44.2$ kPa and $b = 16.7$.

Both the human coronary artery and the rabbit carotid artery are modeled as two-layer vessels, which consider the
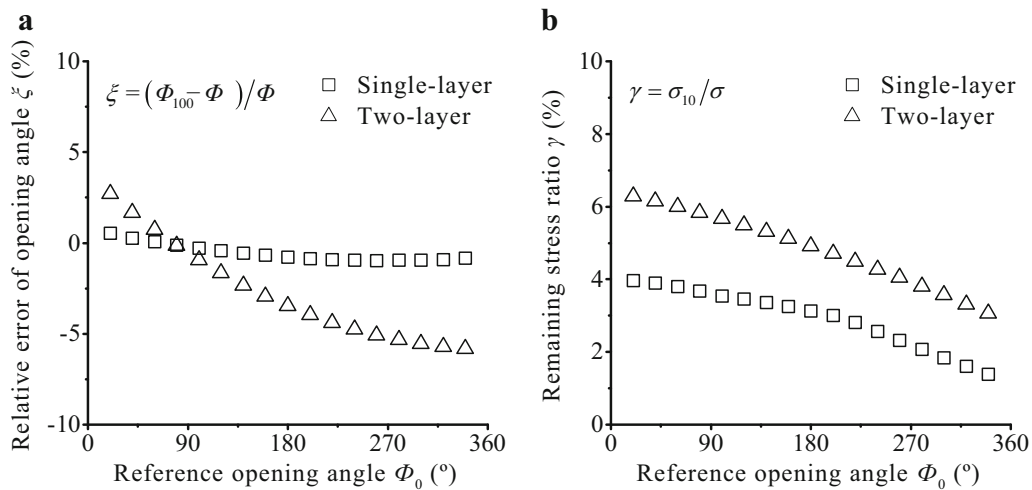
Fig. 4 **a** Relative error of opening angle $\xi = (\Phi_1 - \Phi_0)/\Phi_0$, in which Φ_0 is the reference opening angle, Φ_1 is the simulated opening angle. **b** Remaining stress ratio $\gamma = \sigma_1/\sigma_0$, in which σ_0 and σ_1 are maximum von Mises stress values in the vessels before and after the open-up, respectively. Squares: single-layer model with human carotid constitutive; triangles: two-layer model with rabbit carotid constitutive

media and adventitia layers with the media layer taking 2/3 of the wall thickness [8,16]. The constitutive relation proposed by Holzapfel et al. [16] is adopted as Eq. (11). Here the distortional free-energy functions W_M and W_A to characterize the mechanical behaviors of the media and adventitia, respectively, are adopted

$$W = W_M + W_A, \qquad (11)$$

where

$$W_M = \frac{\mu_M}{2}(\bar{I}_1 - 3)$$
$$+ \frac{k_{1M}}{2k_{2M}} \sum_{i=4,6} \left\{ \exp\left[k_{2M}\left(\bar{I}_{iM} - 1\right)^2 \right] - 1 \right\},$$

$$W_A = \frac{\mu_A}{2}(\bar{I}_1 - 3)$$
$$+ \frac{k_{1A}}{2k_{2A}} \sum_{i=4,6} \left\{ \exp\left[k_{2A}\left(\bar{I}_{iA} - 1\right)^2 \right] - 1 \right\}.$$

Following Gasser et al. [8], we adopt the following parameters for the human coronary artery as $\mu_M = 27$ kPa, $k_{1M} = 0.64$ kPa, $k_{2M} = 3.54$, $\beta_M = 10°$ for the media, and $\mu_A = 2.7$ kPa, $k_{1A} = 5.1$ kPa, $k_{2A} = 15.4$, $\beta_A = 40°$ for the adventitia. The parameters used for the rabbit carotid artery refer to Holzapfel et al. [16], as $\mu_M = 3$ kPa, $k_{1M} = 2.3632$ kPa, $k_{2M} = 0.8393$, $\beta_M = 29°$ for the media, and $\mu_A = 0.3$ kPa, $k_{1A} = 0.562$ kPa, $k_{2A} = 0.7112$, $\beta_A = 62°$ for the adventitia.

Table 3 The classification of blood pressure for adults

Category	Mean systolic P_s(mmHg)	Mean diastolic P_d(mmHg)	Mean pressure $\bar{P}$(mmHg)
Normal	106.0	69.5	81.7
High normal (prehypertension)	129.5	84.5	99.5
Stage 1 hypertension	149.5	94.5	112.8
Stage 2 hypertension	169.5	104.5	126.2
Stage 3 hypertension (hypertensive emergency)	180.0	110.0	133.3

1 mmHg = 1.33 kPa

3.1 Error in residual stress for single and multiple layer models

First, the errors of rebuilt residual stress and opening angles are analyzed with different materials using single-layer or multi-layer blood vessel models. Circumferential residual stress and achieved opening angles after the release of residual stress are compared with referenced results.

Blood vessels are discretized as illustrated in Fig. 2a. For multi-layer vessel models in this study, we assumed that the interface of two layers are bonded together and the displacements for both layers at the interface are identical. To simulate the opening-up process, two separate sets of nodes presenting as *FGHI* surface are created, as shown in Fig. 2b, which works as a preset radial cut along the surface *FGHI* in blood vessels. Node *D* is constrained in all directions to eliminate rigid body motion, all nodes on surface *BCDE* are

constrained in the circumferential direction, and node C is constrained in the radial direction to prevent out-of-plane rotation.

Figure 3 shows the numerical results of the predicted circumferential residual stress for the single-layer (Fig. 3a) and two-layer (Fig. 3b) vessels. The result in Fig. 3a is compared to the semi-analytical solution by solving the boundary value problems based on continuum mechanics [4], and the result for the two-layer model in Fig. 3b is compared to the numerical results from Gasser et al. [8]. Differences in the circumferential stress appear. We believe that this is due to the assumption of isotropic expansion adopted in the thermal approach, with which redundant axial expansion associated with the circumferential expansion was introduced simultaneously. An anisotropic expansion can also be introduced by solving the stress equilibrium equations under thermal-mechanical stress coupling, in which the principal strains and local temperature differences need to be formulated interactively as discussed in Lubarda [22]. However, this generated error of the overall volume change is negligible, as will be discussed later.

The relative error between the given reference opening angle Φ_0 and the opening angle obtained numerically Φ_1, is evaluated as $\xi = (\Phi_1 - \Phi_0)/\Phi_0$. For the single-layer model, the error of the simulated opening angle is 0.21%; for the two-layer model, the error is 0.02% for the media, and 1.45% for the adventitia, respectively.

Table 2 shows the differences of inner and outer radii between the reference and numerical results in the unloaded configuration. The error in relative volume change $\Delta V/V$ is found to be small enough to satisfy the volume conservation.

3.2 Error variation with various reference opening angles

An error sensitivity of the present method to various reference opening angles from 20° to 340° is examined. Figure 4a shows that the relative error of opening angle are less than 1% and 6% for the single-layer and two-layer models, respectively. The residual stress is almost released and the remaining stress ratios for the single-layer and two-layer models are less than 4.0% and 6.3%, as shown in Fig. 4b. The error analysis of the opening-up process indicates that the thermal expansion method could ensure the accuracy of the residual stress rebuilt in blood vessels for a large range of reference opening angles. The experiments by Holzapfel et al. [23] confirmed that an unloaded blood vessel may not release all of the residual stress even it is cut radially and springs open. Nevertheless, the opened-up vessel likely releases most of it [6].
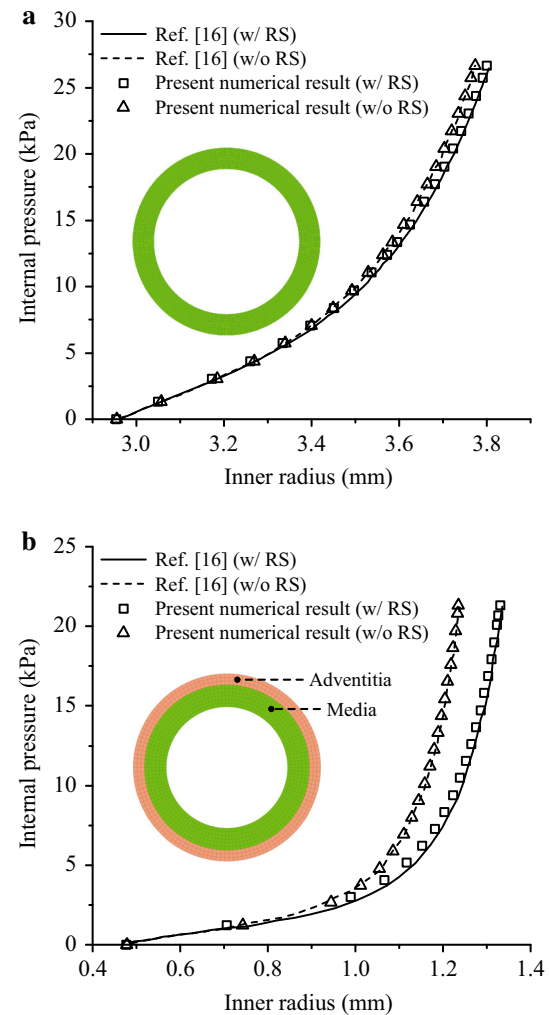
Fig. 5 Comparison of pressure-radius relation of blood vessels between the present numerical results and the reference results in Ref. [16]. **a** Single-layer, human carotid. **b** Two-layer, rabbit carotid. The results with residual stress are labeled as "w/ RS", and those without residual stress are labeled as "w/o RS"

3.3 Validation of the pressure-radius relations

The pressure-radius responding curves with or without the presence of residual stress for the single-layer (Fig. 5a) and two-layer (Fig. 5b) models are compared with results in Ref. [16]. The hyperelastic deformations predicted in the present work agree well with the reference results.

As illustrated by these verification studies, the proposed thermal expansion method is able to apply the residual strain field onto a blood vessel with various given opening angles. Rather than "stitching" the open ends back to a tubular shape numerically as the opening angle method, the proposed method avoids dealing with the large deformation associated with the folding process and eliminates the nonphysical discontinuities of stress distribution acquired by co-localizations in meshes. Instead of managing the residual
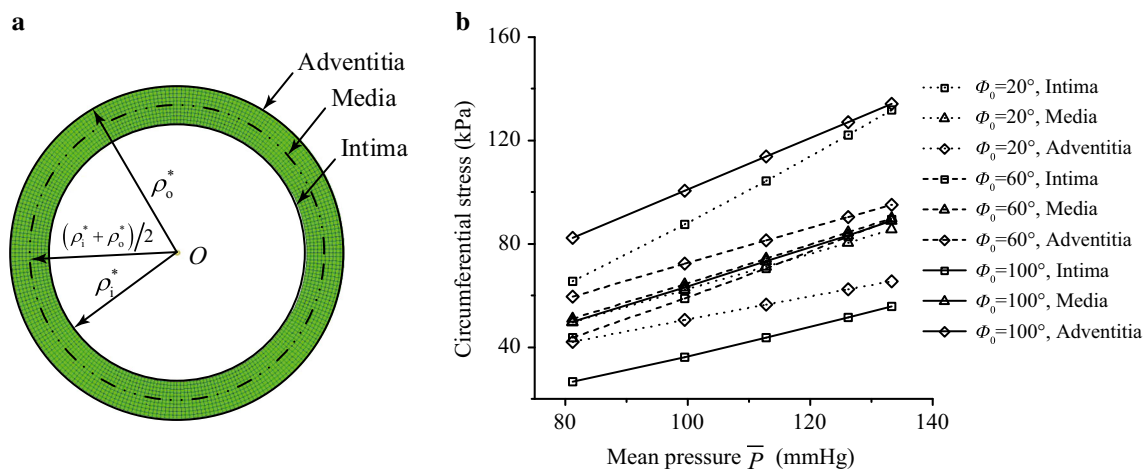
Fig. 6 **a** Single-layer finite element model of a human carotid artery at its virtual state. The intima denotes the inner wall, the media denotes the middle layer, and the adventitia denotes the outer wall. **b** Circumferential stress responses of the intima (square), media (triangle), and adventitia (diamond) under mean blood pressure $\overline{P}$. The data points for $\Phi_0 = 20°, 60°, 100°$ are connected by dotted line, dashed line, and solid line, respectively
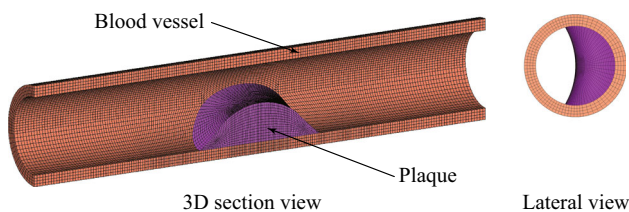
Fig. 7 Stenosed finite element model of a human carotid artery at its virtual state (stenosis 55.52%). The purple mesh presents the plaque with neo-Hookean constitutive, shear modulus $\mu = 100$ kPa. The brown mesh presents the straight blood vessel, single-layer model, the length of the vessel $L = 40$ mm, $\Phi_0 = 100°$, $\rho_i^* = 3.1$ mm, $\rho_o^* = 4.0$ mm, $\lambda_z = 1.1$

strain field iteratively by the volumetric tissue growth method [11] or the scheme used in GPA [14], the present method bypasses the sophisticated iterative process by setting temperature differences explicitly and specifically; therefore, it can be implemented easily and greatly improve the efficiency of the numerical calculation.

4 Applications to hypertension and vascular stenosis

### 4.1 Mechanical stress in different layers of blood vessels under hypertensive pressures

According to Ref. [24] as listed in Table 3, blood pressure is divided into five stages, and each of the stages contains three characteristic pressures, namely, mean diastolic pressure P_d, mean systolic pressure P_s, and the mean pressure $\overline{P}$ determined by $\overline{P} = P_d + (P_s - P_d)/3$.

A single-layer finite element model for the human carotid artery in Table 1 is created for stress analysis. In order to investigate the effect of the variation of residual stress on stress distributions in blood vessels, three different reference opening angles $\Phi_0 = 20°, 60°, 100°$ are adopted, respectively, when casting residual stresses into blood vessels using thermal expansion method. Static blood pressures from normal to hypertensive emergency are inflated into the blood vessels thereafter according to Table 3.

Figure 6a shows different radial locations are selected to represent the intima, media and adventitia layers of blood vessels respectively. The stresses at these three layers represent the stress distributions of endothelial cells (ECs), vascular smooth muscle cells (VSMCs), and cells in tissues at the outside boundaries of the blood vessels.

The circumferential stresses in the blood vessels are predicted as shown in Fig. 6b. For all opening angles adopted, an increase of blood pressure results in an increase of circumferential stress in each layer. The most obvious increase of the circumferential stress in blood vessels appears in the intima layer where ECs locate. While the mean pressure increases 63% (i.e. from 81.7 to 133.3 mmHg), the maximum increase of the stress in the intima layer varies from 101.2% to 110.0%. Although the increase of the circumferential stress for each layer is enhanced by the increase of opening angle, we find that when the opening angle increases five times from 20° to 100°, the maximum stress increases in different vessel layers associated with the blood pressure increase are limited from 8.75% (for the intima) to 12.3% (for the adventitia), which indicates that an apparent nonlinear dependence of the blood inflation induced stress increase on the residual stress embedded in the vessels. As shown in Fig. 6b, with the increase of the opening angle Φ_0, the circumferential stress
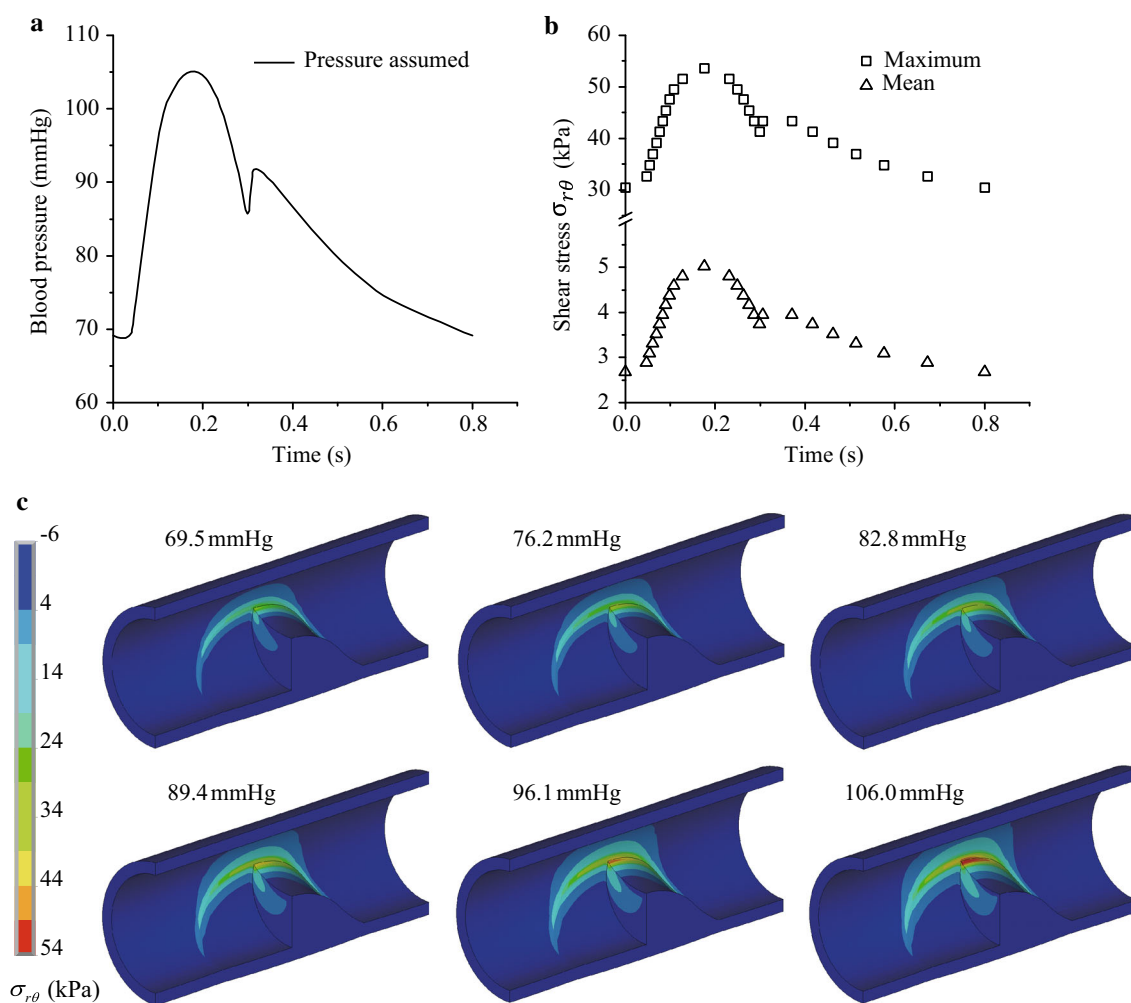
Fig. 8 **a** Normal blood pressure profile simply assumed. **b** Variations of the maximum and mean of the elastic shear stress $\sigma_{r\theta}$ in the plaque during a cardiac cycle of plot **a**. **c** Elastic shear stress $\sigma_{r\theta}$ distribution in the stenosed vessel under normal blood pressure ranging from 69.5 to 106.0 mmHg. Only the middle part containing the plaque is shown; the length of the vessel is $L = 20$ mm. Considering the geometrical symmetry, it shows half of the artery and a quarter of the plaque

of the intima decreases while the adventitia increases. Specifically, the stresses of the media layers (labeled as triangles in Fig. 6b) coincide with each other for all opening angles, which suggests that the variation of the residual stress has minor influence on the stress in the media layer.

Figure 6b also shows that under the residual stress when Φ_0 equals 60°, the circumferential stress has the minimum amount of variation along the radial direction compared to the cases of 20° and 100°. This suggests that in order to ensure homogeneous stress distribution, the opening angle is a specific value when the blood pressure is given. We know that when the blood pressure becomes abnormal, the stress-modulated remodeling of the vascular tissue adjusts the stress distribution in the blood vessel and the opening angle also changes [25]. As shown in the present work, optimal residual stresses maintaining a uniform stress distribution can

be predicted and used for estimating the mechanobiological variations when the blood pressure alters.

4.2 Variation of mechanical stress around stenosis during a cardiac cycle

The variations of stress in plaques are studied using the thermal expansion method. Figure 7 shows a discretized mesh of a stenosed human carotid artery. The plaque is modeled as neo-Hookean material with the shear modulus $\mu = 100$ kPa [26]. The length of the vessel wall adopted is ten times of the outer radius so that the influences from the ends constraints are negligible. Both plaque and blood vessel are simplified as ideal geometries with smooth surfaces.

For stenosed vessels, the discontinuity of the material property between the plaque and vessel wall often causes additional elastic shear stress. During a cardiac cycle

(Fig. 8a), the maximum of elastic shear stress $\sigma_{r\theta}$ in the plaque varies from 30.5 to 53.6 kPa, and the mean value varies from 2.7 to 5.0 kPa (Fig. 8b). The elastic shear stress $\sigma_{r\theta}$ distribution in the stenosis is shown in Fig. 8c. It is found that high elastic shear stress $\sigma_{r\theta}$ appears on the edge of the plaque, which forms an arched zone. The maximum elastic shear stress $\sigma_{r\theta}^{\max}$ is located at the shoulder of the plaque. Figure 8b, c suggests that both the area of arched zone and the maximum $\sigma_{r\theta}^{\max}$ experience a periodic fluctuation under every pulse, which functions as a "tearing effect". This "tearing effect" may explain the fatigue rupture that appears at the shoulder of plaques as observed by Li et al. [27] in their clinical studies.

Moreover, the maximum value $\sigma_{r\theta}^{\max}$ increases by 76% when the blood pressure climbs to 106.0 mmHg (Fig. 8b), which is about 1.2 times the circumferential stress of intima of healthy vessels. It indicates that large elastic shear stress $\sigma_{r\theta}$ appears around the plaque for each cardiac cycle, which supports the use of $\sigma_{r\theta}$ as a key index when evaluating the risk of plaque rupture.

5 Conclusions

In this work, a thermal expansion method was developed for numerical study of in vivo mechanical stress in blood vessels under healthy and pathological conditions. The results of present method provide good agreements with the reference results of the opening-up processes and the pressure-radius relations. The robust solutions in rebuilding residual stresses for blood vessels with a large range of reference opening angles are also presented. It is found that the present method is easy to apply with the multi-layer model of blood vessels for various constitutive relations. The developed numerical procedure based on thermal expansion method is competent for further in vivo stress prediction of pathological blood vessels under different physiological conditions. In addition, numerical results showed that the most obvious increase of the circumferential stress appears in the intima layer while pressure increases from normal blood pressure to severe hypertension, and also suggested that specific residual stresses ensuring a uniform stress distribution can be predicted for given blood pressures. Furthermore, a case study of in vivo stress estimation of a plaque in a vessel during a cardiac cycle supported that the elastic shear stress around the shoulder could be taken as a key index when evaluating the rupture risk because of the "tearing effect".

References

1. Humphrey, J.D.: Vascular adaptation and mechanical homeostasis at tissue, cellular, and sub-cellular levels. Cell Biochem. Biophys. **50**, 53–78 (2008)
2. Wang, G.L., Wang, L.Y., Yang, S.X., et al.: Arterial wall remodeling under sustained axial twisting in rats. J. Biomech. **60**, 124–133 (2017)
3. Cyron, C.J., Humphrey, J.D.: Growth and remodeling of load-bearing biological soft tissues. Meccanica **52**, 645–664 (2017)
4. Humphrey, J.D.: Cardiovascular Solid Mechanics: Cells, Tissues, and Organs. Springer, New York (2002)
5. Chuong, C.J., Fung, Y.C.: Three-dimensional stress distribution in arteries. J. Biomech. Eng. **105**, 268–274 (1983)
6. Han, H.C., Fung, Y.C.: Direct measurement of transverse residual strains in aorta. Am. J. Physiol. **270**, H750–H759 (1996)
7. Delfino, A., Stergiopulos, N., Moore, J.E., et al.: Residual strain effects on the stress field in a thick wall finite element model of the human carotid bifurcation. J. Biomech. **30**, 777–786 (1997)
8. Gasser, T.C., Schulze-Bauer, C.A.J., Holzapfel, G.A.: A three-dimensional finite element model for arterial clamping. J. Biomech. Eng. **124**, 355–363 (2002)
9. Ohayon, J., Dubreuil, O., Tracqui, P., et al.: Influence of residual stress/strain on the biomechanical stability of vulnerable coronary plaques: potential impact for evaluating the risk of plaque rupture. Am. J. Physiol. Circ. Physiol. **293**, H1987–H1996 (2007)
10. Fereidoonnezhad, B., Naghdabadi, R., Holzapfel, G.A.: Stress softening and permanent deformation in human aortas: continuum and computational modeling with application to arterial clamping. J. Mech. Behav. Biomed. Mater. **61**, 600–616 (2016)
11. Polzer, S., Bursa, J., Gasser, T.C., et al.: A numerical implementation to predict residual strains from the homogeneous stress hypothesis with application to abdominal aortic aneurysms. Ann. Biomed. Eng. **41**, 1516–1527 (2013)
12. Fung, Y.C.: What are the residual stresses doing in our blood vessels? Ann. Biomed. Eng. **19**, 237–249 (1991)
13. Weisbecker, H., Pierce, D.M., Holzapfel, G.A.: A generalized pre-stressing algorithm for finite element simulations of preloaded geometries with application to the aorta. Int. J. Numer. Methods Biomed. Eng. **30**, 857–72 (2014)
14. Pierce, D.M., Fastl, T.E., Rodriguez-Vila, B., et al.: A method for incorporating three-dimensional residual stretches/stresses into patient-specific finite element simulations of arteries. J. Mech. Behav. Biomed. Mater. **47**, 147–164 (2015)
15. Holzapfel, G.A., Mulvihill, J.J., Cunnane, E.M., et al.: Computational approaches for analyzing the mechanics of atherosclerotic plaques: a review. J. Biomech. **47**, 859–869 (2014)
16. Holzapfel, G.A., Gasser, T.C., Ogden, R.W.: A new constitutive framework for arterial wall mechanics and a comparative study of material models. J. Elast. **61**, 1–48 (2000)
17. Ross, R.: The pathogenesis of atherosclerosis: a perspective for the 1990s. Nature **362**, 801–809 (1993)
18. Gimbrone, M.A., García-Cardeña, G.: Endothelial cell dysfunction and the pathobiology of atherosclerosis. Circ. Res. **118**, 620–636 (2016)
19. Barrett, H.E., Cunnane, E.M., Kavanagh, E.G., et al.: On the effect of calcification volume and configuration on the mechanical behaviour of carotid plaque tissue. J. Mech. Behav. Biomed. Mater. **56**, 45–56 (2016)

20. Cunnane, E.M., Mulvihill, J.J.E., Barrett, H.E., et al.: Mechanical properties and composition of carotid and femoral atherosclerotic plaques: a comparative study. J. Biomech. **49**, 3697–3704 (2016)

21. Demiray, H.: A note on the elasticity of soft biological tissues. J. Biomech. **5**, 309–311 (1972)

22. Lubarda, V.A.: Constitutive theories based on the multiplicative decomposition of deformation gradient: thermoelasticity, elasto-plasticity, and biomechanics. Appl. Mech. Rev. **57**, 95–108 (2004)

23. Holzapfel, G.A., Sommer, G., Auer, M., et al.: Layer-specific 3D residual deformations of human aortas with non-atherosclerotic intimal thickening. Ann. Biomed. Eng. **35**, 530–545 (2007)

24. Chobanian, A.V., Bakris, G.L., Black, H.R., et al.: Seventh report of the Joint National Committee on prevention, detection, evaluation, and treatment of high blood pressure. J. Am. Heart Assoc. **42**, 1206–1252 (2003)

25. Fung, Y.C., Liu, S.Q.: Change of residual strains in arteries due to hypertrophy caused by aortic constriction. Circ. Res. **65**, 1340–1349 (1989)

26. Barrett, S.R.H., Sutcliffe, M.P.F., Howarth, S., et al.: Experimental measurement of the mechanical properties of carotid atherothrombotic plaque fibrous cap. J. Biomech. **42**, 1650–1655 (2009)

27. Li, Z.Y., Howarth, S., Trivedi, R.A., et al.: Stress analysis of carotid plaque rupture based on in vivo high resolution MRI. J. Biomech. **39**, 2611–2622 (2006)